Recent advances on innovative bioactive glass-hydroxyapatite composites for bone tissue applications: Processing, mechanical properties, and biological performance

Damiano Angioni [a], Roberto Orrù [a,*], Giacomo Cao [a], Sebastiano Garroni [b], Devis Bellucci [c], Valeria Cannillo [c]

[a] *Dipartimento di Ingegneria Meccanica, Chimica, e dei Materiali, Unità di Ricerca del Consorzio Interuniversitario Nazionale per la Scienza e Tecnologia dei Materiali (INSTM), Università degli Studi di Cagliari, via Marengo 2, 09123 Cagliari, Italy*
[b] *Dipartimento di Scienze Chimiche, Fisiche, Matematiche e Naturali, Università degli Studi di Sassari, Via Vienna 2, 07100 Sassari, Italy*
[c] *Dipartimento di Ingegneria "Enzo Ferrari", Università di Modena e Reggio Emilia, Via P. Vivarelli 10, 41125 Modena, Italy*

ARTICLE INFO

ABSTRACT

New Hydroxyapatite-Bioactive Glass composites, xHA-(1-x)BG (x = 25, 50, and 75 wt %), are developed using HA and BGMS10 glass powders co-milled up to 2 h prior to Spark Plasma Sintering (SPS). Ball milling (BM) promoted the consolidation of HA-rich powders, whereas hindered the densification of 25HA-75BG samples. HA crystallite size is reduced from > 200 nm (unmilled) to 60 (x = 25 %) or 88 nm (x = 75 %) when using 2 h milled mixtures. Glass crystallization occurred in 75HA-25BG samples processed by SPS at 950 °C: a negligeable effect in the amount of the residual amorphous phase (12.3–13.3 wt %) is produced by BM, while changes are observed in the relative content of crystalline phases, with SiO_2 increases from 8.5 to 13.1 wt %, whereas α- and β-$CaSiO_3$ correspondingly decrease. Superior Young's modulus and Vickers hardness (130 GPa and 726, respectively) are obtained in HA rich products. Biological tests evidenced that the milling treatment does not determine negative consequences on cells viability.

1. Introduction

During the past decades, significant advances have been achieved in the development of bioactive ceramics, such as hydroxyapatite (HA), tricalcium phosphates (TCP), etc., and glasses, which provided a valuable contribution in the biomedical field, particularly for orthopaedic applications [1,2]. In this context, despite its good biocompatibility and osteoconductivity, stoichiometric HA ($Ca_{10}(PO4)_6(OH)_2$) is also known to be biologically stable under physiological conditions [1]. This entails that its interaction with biological fluids, the consequent release of calcium and phosphate ions, as well as the formation of a stable chemical bond between the bone and the material, occur too slowly. On the other hand, such physico-chemical phenomena can be promoted if less stable calcium phosphates (calcium-deficient hydroxyapatite, tricalcium-phosphate, amorphous calcium phosphates, etc.) are used instead of the stoichiometric compound [1]. Alternatively, HA can be combined in suitable proportions with more reactive secondary phases, particularly bioactive glass (BG) formulations. Indeed, due to their amorphous nature, BGs undergo rapid degradation when exposed to physiological fluids. As a result, the formation of a superficial film of hydroxycarbonate apatite (HCA) occurs at a relatively faster rate, effectively promoting the subsequent bonding process with natural bone. In principle, the release rate of ions can be then properly tailored by varying the fraction of each constituent in the HA-BG composite system. The introduction of the BG phase often improves, other than the undesired slower resorption kinetics of HA, also its usually modest mechanical properties.

The considerations above have prompted several research groups to the development of novel HA-BG composites with improved performances [3–18]. For instance, sintered disks (1200–1350 °C, 1 h) resulting from the combination of HA and $CaO-P_2O_5$ types of glass have shown to exhibit better mechanical properties, compared to the additive free ceramics [3–5]. In addition, the bioactive behaviour of these samples was testified by the formation of a carbonated apatite layer when immersed in Hank's balanced salt solution [6].

In recent years, two novel bioactive glasses with low tendency to

---

* Corresponding author.
E-mail address: roberto.orru@unica.it (R. Orrù).

crystallize, namely BG_Ca/Mix and BGMS10, were coupled in different proportions with commercial HA to form bulk composites by pressure-less [8,9,11] or Spark Plasma Sintering (SPS) [10,16,18–20]. BGMS10 (composition: 2.3 % Na_2O, 2.3 % K_2O, 25.6 % CaO, 10.0 % MgO, 10.0 % SrO, 2.6 % P_2O_5 and 47.2 % SiO_2, mol %) [20] takes the already promising BG_Ca/Mix glass (2.3 % Na_2O, 2.3 % K_2O, 45.6 % CaO, 2.6 % P_2O_5 and 47.2 % SiO_2, mol %) [21] and further enhances its perfor-mance in terms of both biological activity and thermal stability. BGMS10 boasts an impressive crystallization temperature of 932 °C, which is believed to be one of the highest reported in bioactive glass literature. This glass exhibits an exceptionally low tendency to crystal-lize, allowing successful sintering at relatively low temperatures (approximately 740 °C). This unique characteristic preserves its amor-phous nature and, consequently, may favour the optimal release of ions both in vitro and in vivo. The thermal stability of BGMS10, compared to the "gold" standard 45S5 Bioglass® that crystallizes between 650 °C and 690 °C [22], can be attributed to several factors. Firstly, its low content of alkaline oxides reduces the glass structural mobility at high temper-atures, thereby hindering devitrification. Secondly, by incorporating K^+ ions instead of the more commonly used Na^+ ions among the alkaline oxides, the BGMS10 further reduces structural mobility at elevated temperatures due to the larger size of K^+ ions relative to Na^+ ions. Lastly, the potential inhibitory effect of MgO on crystallization might further contribute to the thermal stability of BGMS10, although the scientific community continues to debate this topic [20]. Additionally, BGMS10 shows great promise from a biological standpoint thanks to the presence of strontium and magnesium ions, whose biological role is well-documented in the existing literature [23,24].

By utilizing SPS, it has been made possible to sinter the aforemen-tioned glasses with HA, leading to significantly enhanced consolidation levels and mechanical properties when compared to traditional sintering methods. The capability of the SPS technology to successfully produce HA-BG_Ca/Mix based Functionally Graded Materials (FGMs) was also demonstrated [16]. More recently, the effect produced by a ball milling (BM) treatment on 50HA-50BGMS10 composite powders (wt %) prior their consolidation by SPS was investigated [18]. A 30 min long treat-ment was found to provide an improvement, with respect to unmilled samples, of the mechanical properties (Young's Modulus and Vickers Hardness) as well as a significant enhancement of the apatite-forming ability of the composite material during in-vitro tests in SBF.

In the present work, the previous study is extended to the 25HA-75BG and 75HA-25BG (wt %) compositions, still using BGMS10 glass as BG constituent. The effect of the sintering temperature and the applied pressure during the consolidation by SPS of unmilled powders was first systematically investigated. A mechanical treatment of the composite mixtures is then performed for different time intervals, to evaluate if the resulting samples densification, mechanical, and in vitro biological behaviour are affected.

2. Experimental procedure

2.1. Processing and characterization of composite powders

Three formulations of the xHA-(1-x)BG composite system (x = 25, 50, and 75 wt %) were investigated starting from commercial HA (Plasma Biotal Ltd., UK; Cod. CAPTAL 60–1; 1.67 Ca/P ratio, 99 % pu-rity, 99 % crystallinity) and BGMS10 lab-made bioactive glass (particle size < 63 μm) powders. Details on the glass preparation are reported elsewhere [20]. The two-components powder batches were dry mixed in air using a SPEX 8000 (SPEX CertiPrep, USA) shaker mill, plastic vials and small agata balls (7 mm diam.). The possible effect produced by a mechanical treatment on the HA-BGMS10 mixtures was investigated by ball milling about 2.4 g of the composite powders for different time intervals (t_{BM}= 30, 60, and 120 min) using the SPEX 8000 device mentioned above, equipped with agata milling tools (two balls, 12 mm diam.). The ball-to-powder weight ratio was set to 2.

Phase compositions and microstructural features were determined by X-ray diffraction analysis (Philips PW 1830, Netherlands). Data were acquired using a Cu Kα radiation in the 2θ range of 20°–130°, steps of 0.05° with 15 s acquisition time per angle. XRD patterns were processed using the Rietveld method (MAUD software) to estimate phases amount and the corresponding microstructural parameters [25]. The glass phase has been computed using a pseudo-crystalline structure factor ($Ca_{1.5}Na_{2.64}Si_9O_3$ phase; symmetry: trigonal; space group: R-3 m; crystallite size: 20 Å; microstrain: 0.03) according to the LeBail approach [26].

The particle size distribution of the composite powders subjected to the different milling conditions was provided by laser light scattering analysis (CILAS 1180, France).

The specific surface area was measured by N_2 sorption technique by a Sorptomatic 1990 instrument (Fisons Instruments, Milan, Italy) and calculated according to the BET method. To this aim, 600 mg of each sample were degassed in a quartz tube under 100 Pa at 180 °C for 24 h, while the dead volume of the quartz tube was evaluated through helium adsorption measurements.

2.2. Powder sintering and characterization of composite samples

The differently milled HA-BGMS10 mixtures were loaded in a graphite die (Atal Srl., Italy; 15 mm inner diameter; 35 mm external diameter; 40 mm height) and then consolidated by SPS (515 S model, Fuji Electronic Industrial Co., Ltd., Kanagawa, Japan) under vacuum conditions. During SPS, the temperature was measured by a K-type thermocouple (TC Misure e Controlli S.R.L., Italy) inserted into a small hole drilled on the external surface of the die. The first non-isothermal stage consisted of sample heating at a rate of 50 °C/min until 100 °C below the dwell temperature (T_D) was reached. The heating rate was then decreased to 10 °C/min, to reduce possible overshooting problems while approaching the T_D value. After the isothermal holding for 2 min at the maximum temperature, the sample was cooled to 300 °C at a rate of 50 °C/min, followed by a natural cooling step. The dwell temperature and the applied pressure (P) were varied, depending on the relative fraction of the two composite constituents, in the range 700–1200 °C and 16–70 MPa, respectively. Further details on the SPS procedure can be found elsewhere [18].

Sintered products were ground using abrasive papers to remove re-sidual graphite from their surface. Samples of about 14.7 mm diameter and 2.5 mm height were finally obtained. Each experimental condition was replicated at least twice.

Densities were determined by the Archimedes' method using ethanol as immersing medium and an analytical balance (Ohaus Explorer Pro, Ohaus Corporation, NJ, USA) (± 0.0005 g precision). The theoretical densities of each system were evaluated on the basis of a rule of mixture [27] and considering the values of 3.16 and 2.97 g/cm³ [28] for HA and BGMS10, respectively.

2.3. Mechanical properties

The Young's modulus and the hardness of the resin-embedded and mirror-polished samples were evaluated using the micro-indentation technique. The measurements were performed using Open Platform equipment from CSM Instruments (Peseux, Switzerland) with a Vickers indenter tip. A load of 500 mN was applied during the indentation process, with a loading/unloading rate of 1 N/min (loading time at maximum load: 15 s). At least fifteen measurements were taken for each sintered disk, and the load-penetration depth curve was automatically recorded for each indentation. The elastic modulus was then calculated using the Oliver and Pharr method based on the indentation load-unloading curves [29].

2.4. Biological tests

The cytotoxic potential of the produced composites was evaluated

using an indirect contact method, which involves culturing cells in an eluate produced from the samples. Before conducting the tests, all materials were placed in Petri dishes and sterilized using UV light for 1 h on each side to ensure their sterility. To obtain extracts, the samples were placed in centrifuge tubes containing culture medium (DMEM - Dulbecco's modified Eagle's medium, Euroclone, Milan, Italy. A ratio of 1 ml of DMEM per 3 cm^2 of sample surface area was employed). A vial with DMEM and latex glove solution (prepared with the same 3 cm^2/1 ml ratio) served as the positive control, while a vial with DMEM only was used as the negative control. Vials were incubated at 37 °C for 3 days (NS 9060llx-ISCO, Italy). Prior to the cytotoxicity test, each extract was filtered through a 0.22-micron filter.

MLOY04 cells (murine long bone osteocyte Y4) were propagated as indicated by the supplier using DMEM supplemented with 10 % foetal bovine serum (Euroclone) and penicillin-streptomycin solution (Euroclone). The cells were cultured in 96-well plates containing the samples' extracts and maintained in an incubator at 37 °C ± 1 °C, 5.0 % ± 1 % CO$_2$/air and 90 % ± 5 % humidity. Cells viability was investigated after 24 and 72 h by using the alamar-Blue® Cell Viability Reagent assay (Thermo Fisher Scientific), a redox indicator that measures

quantitatively cell proliferation. The alamar-Blue® reagent diluted 1:10 was added to the culture and incubated. The plates were read in absorbance at an excitation wavelength of 570 nm after 6 h of incubation. Percent cell viability was expressed by the absorbance count of the negative control compared with the eluate-treated samples.

3. Results and discussion

3.1. Powders processing and characterization

Fig. 1 shows the effect produced by the ball milling treatment on the particle size distribution of 25HA-75BG and 75HA-25BG mixtures. Data relative to the 50HA-50BG composition are available in Angioni et al. [18]. The corresponding d10, d50, d90, and d43 parameters are reported in supplementary Table S1. The BM treatment is found to affect differently the processing powders, depending on the relative amount of the two constituents. The unmilled 25HA-75BG mixture displays a tri-modal q3 distribution (black line in Fig. 1(b)), with the three groups of particles associated to sizes of about 1.5, 7, and 20 μm, respectively. The 30 min long mechanical treatment determined a decrease of the
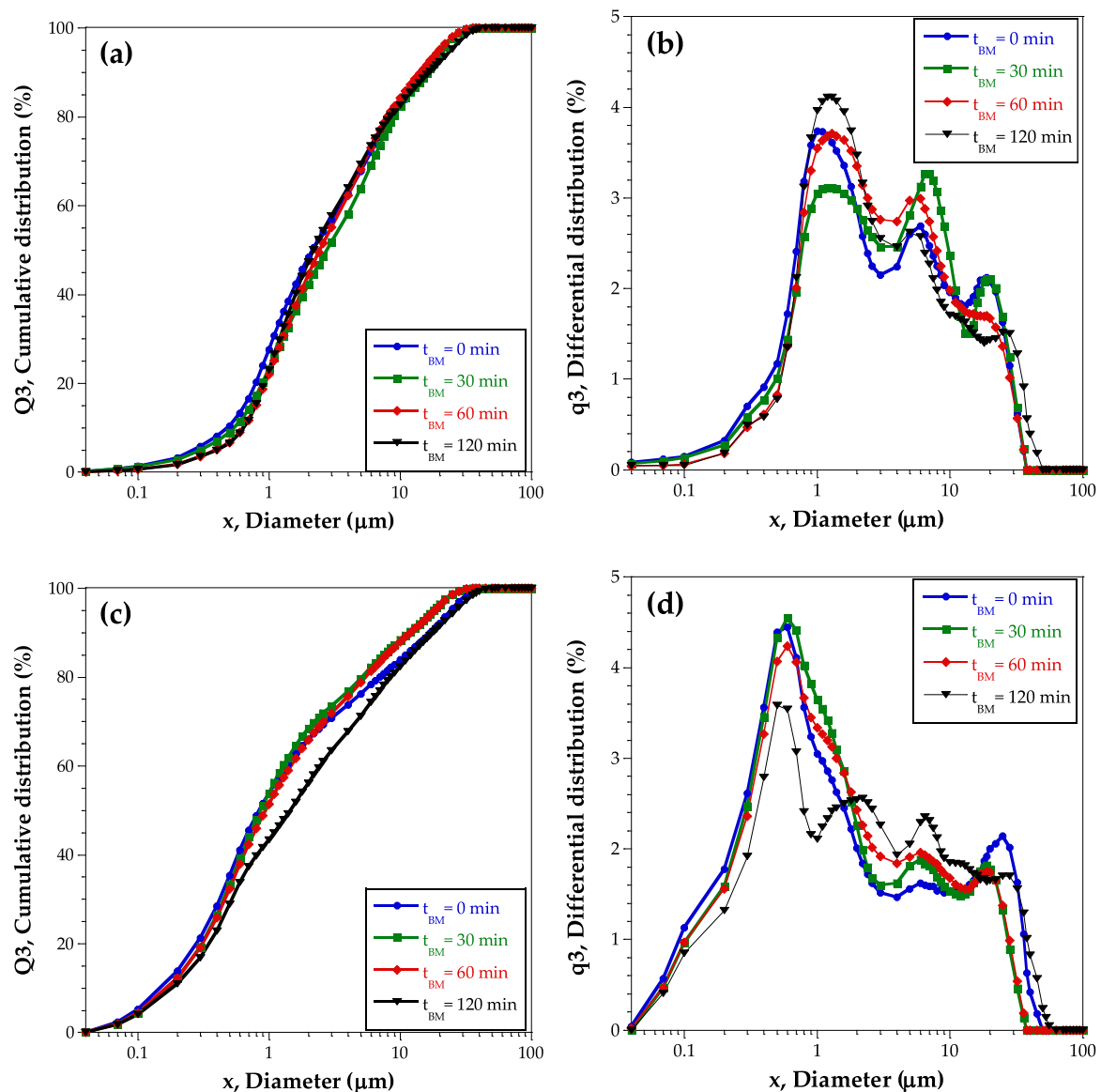

Fig. 1. Effect of the milling time on the particles size distribution (cumulative and differential curves) of (a)-(b) 25HA-75BG and (c)-(d) 75HA-25BG powder mixtures.

fraction of finer powders (1.5 μm) and, concurrently, an increase of that corresponding to those 7 μm sized (green line in Fig. 1(b)). Particles agglomerate during such milling time interval, as also confirmed by the slight increase of their average size (d43 parameter) from 5.3 to 5.8 μm (Table S1). A reverse behaviour was encountered when the milling time was prolonged to 60 (red curves) and 120 min (black curves), with a decrease of both classes of larger sized particles (7 and 20 μm). Thus, during long milling treatments, comminution phenomena prevail in BG-rich composite powders to generate finer particles with average size of 4.5 μm (Table S1).

When considering the 75HA-25BG mixture (Fig. 1(c)-(d)), BM treatments up to 60 min duration did not produce noteworthy changes, particularly on smaller particles. However, as the milling time was extended to 120 min, the intensity of the peak at 0.6 μm of the q3 curve decreases, whereas that of 7 μm sized class of powder correspondingly increases (black line in Fig. 1(d)). In addition, a new class of particles with size in the 2–3 μm range is formed.

Based on the results described above, and those arising from our previous study focused on the 50HA-50BG formulation [18], it is possible to state that agglomeration mechanism usually prevails during ball milling of composite mixtures with 50 wt % or higher contents of HA. Conversely, when processing the composite mixture rich in BG (25HA-75BG), particles coarsening plays a major role only in the 0–30 min milling time range, whereas, as the mechanical treatment is prolonged, comminution phenomena are highly favoured by the presence of larger fraction of the hard/fragile BG phase.

Possible changes in the specific surface areas of 25HA-75BG and 75HA-25BG mixtures as a function of milling time have been investigated by N_2 physisorption. The isotherms of all samples are shown in Fig. S1, while the specific surface areas estimated according to the B.E.T equation, have been reported in Fig. 2.

As for the N_2 isotherms relative to the 50HA-50BG investigated in a previous work [18], also the two new formulations considered here show a type II isotherm with a H3 type hysteresis loop typical of macroporous materials. For both mixtures, the specific surface areas highly increased after the mechanical treatment. In particular, the maximum surface area values are achieved when $t_{BM} = 120$ (16.1 m^2 g^{-1}) and 60 min (19.3 m^2 g^{-1}) for the composite systems richer in HA and BG respectively. On the other hand, within the milling conditions adopted in this work, 30 min of treatment seems to be enough to guarantee the most significant enhancement of this parameter for both composite formulations. This also agrees with the behaviour displayed by the 50HA-50BG system [18].

The XRD patterns of 25HA-75BG and 75HA-25BG powders ball milled for different time intervals are reported in Fig. 3(a) and (b), respectively. The corresponding microstructural parameters and the relative amount of each phase, evaluated using the Rietveld procedure, are listed in Tables S2 and S3. Hydroxyapatite (S.G. P63/m) and an amorphous phase, ascribed to the BGMS10 glass, are the only constituents detected by XRD analysis, regardless the composite formulation and the mechanical treatment condition. The estimated amounts of HA and BGMS10 in the two composite powders, i.e., 23/77 and 74/26 (wt %) (Tables S2-S3), are both very close to their nominal values. Hydroxyapatite crystallites size in 25HA-75BG decreased significantly from >200 to 71 nm (Table S2), after only 30 min ball milling. As the treatment was extended to 60 and 120 min, a further HA crystallite size refinement was obtained, i.e., 59 and 44 nm, respectively.

Similar outcomes resulted when considering the other composite mixture, richer in HA. Indeed, the 2 h duration mechanical process induced the progressive reduction of the crystallite size of the latter phase from >200 nm (unmilled) to about 53 nm (t_{BM}=120 min). Such results are also consistent to experimental findings reported in our recent study focused on the 50/50 (wt %) composite [18]. In the latter investigation, the HA crystallite size at $t_{BM} = 120$ min was found to be equal to about 47 nm, i.e. in between to the values of 44 and 53 nm obtained for the 25HA-75BG and 75HA-25BG systems, respectively. A superior crystallite size refinement is also observed at shorter milling intervals, when considering BGMS10-rich composites. For instance, 59 (75 % BG) instead of 79 nm (25 % BG) sized HA crystallites were obtained at $t_{BM} = 60$ min. This holds also true at t_{BM}= 30 min. Such findings allow us to state that the milling treatment becomes more effective as the fraction of the hardest glass phase in the composite is predominant.

3.2. Bulk composite samples

3.2.1. Densification behaviour

Fig. 4(a)-(b) show the dependence of the relative density of 25HA-75BG and 75HA-25BG samples obtained by SPS from unmilled powders on the holding temperature and the applied pressure, respectively. Literature data relative to individual BGMS10 [28] and 50HA-50BG composite [18] are also reported, for the sake of comparison. When pure glass powders were processed, the sintered samples obtained at P = 16 MPa (Fig. 3(a)) displayed their highest consolidation level at
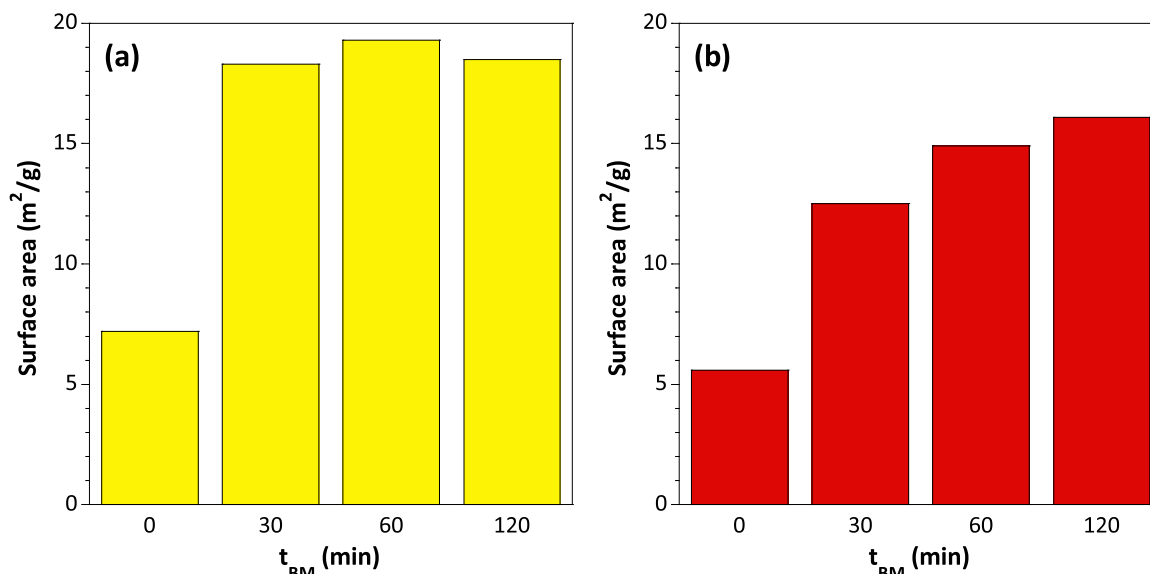
Fig. 2. Specific surface area values of (a) 25HA-75BG, and (b) 75HA-25BG samples obtained for different ball milling times (related isotherms are shown Fig. S1).
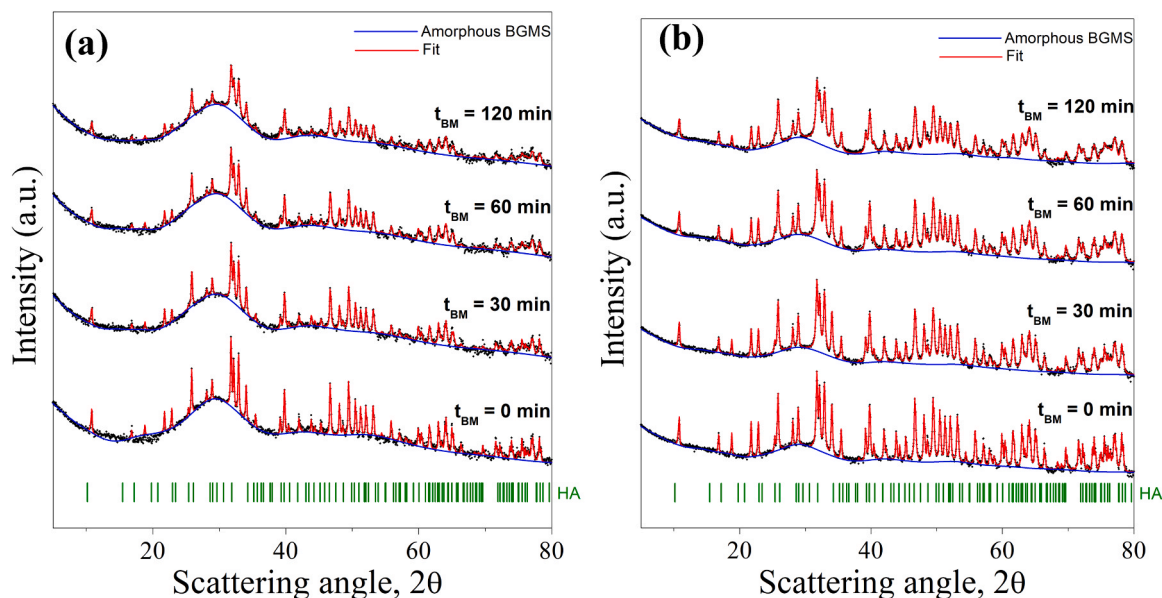
Fig. 3. XRD patterns of differently milled (a) 25HA-75BG and (b) 75HA-25BG powders. Black dots are experimental data, and the red line is the calculated fit. Amorphous BGMS10 profile is indicated by the blue full line.
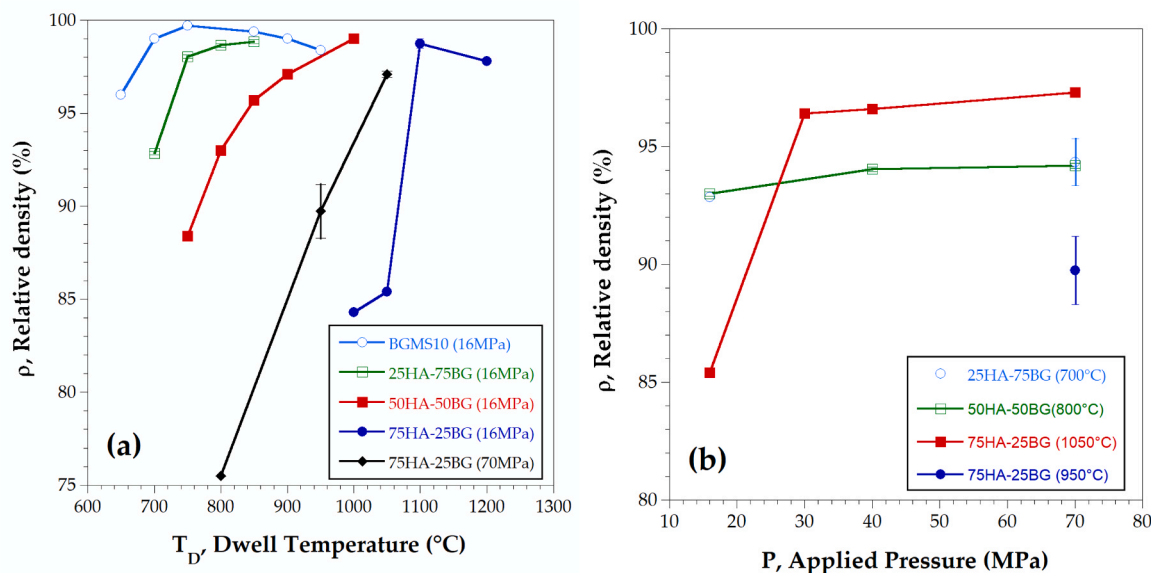

Fig. 4. Effect of (a) the sintering temperature and (b) the applied pressure on the relative density of 25HA-75BG and 75HA-25BG bulk samples produced by SPS from unmilled mixtures (t_{BM} = 0 min). Data of pure BGMS10 [28] and 50HA-50BG [18] are also plotted for comparison.

T_D= 750 °C [28]. A further increase of the temperature promoted the glass crystallization and, in turn, a slight density decrease [28]. As expected, the introduction of progressively higher amounts of HA to the glass makes the resulting composite mixture more difficult to densify. A significant improvement (from 92.9 % to 98.1 % relative density) is observed for the 25HA-75BG system when the temperature was raised from 700° to 750°C (Fig. 4(a), green line). An additional increase in the density, albeit at a lower rate, was achieved with a further temperature increment. The maximum consolidation level (98.9 %) was obtained at 850 °C. The application of higher pressures (from 16 to 70 MPa) was found to produce only a slight enhancement in 25HA-75BG samples densities, i.e., from 92.9 % to 94.4 %, when operating at T_D = 700 °C.

As the fraction of HA in the composite is increased to 50 wt %, the corresponding powders are scarcely consolidated at 750 °C/16 MPa (relative density of about 88.4 %). However, as the temperature was

progressively raised to 850, 900, and 1000 °C (P = 16 MPa), the resulting sintered samples were 95.9 %, 97.1 % and 99 % dense, respectively.

From Fig. 4(b), it is seen that, when the mechanical pressure was increased from 16 to 70 MPa, the densification behaviour shown at 800 °C by 50HA-50BG powders is very similar to that displayed by the 25HA-75BG system at 700 °C, with a moderate improvement in sample compactness (from 93 % to 94.2 %).

The presence of a superior HA percentage in the composite required the use of higher temperatures to reach adequate relative density levels by SPS. Indeed, the densification at 1000 or 1050 °C of the 75HA-25BG mixture led to poorly densified products, with densities of 84.3 % and 85.4 % (Fig. 4(a), blue line), respectively. In contrast, a significant beneficial effect is obtained at 1100 °C, with final densities equal to 98.8 %. A further temperature increase produced broken samples, also

characterized by lower density (97.8 %).

The effect of the applied pressure on the densification of 75HA-25BG powders is quite interesting (Fig. 4(b), red line). Differently from the other two composite formulations, in this case pressure was observed to have a marked effect on the sintering process, causing an increase of bulk sample's density from 85.4 % to 96.4 %, when this parameter was raised from 16 to 30 MPa, respectively. An additional slight improvement in powder densification was achieved when the applied pressure was raised to 70 MPa (97.3 %). Owing to the latter result, and with the aim of possibly mitigating the temperature condition for achieving suitable densification levels, the effect of the dwell temperature for the 75HA-25BG system was also examined when P = 70 MPa (Fig. 4(a), black line). Under the latter condition, the poor densification obtained at 800 °C (75.5 %) was highly improved at 950 °C (89.7 %) and, above all, at 1050 °C (97.3 %).

The three composite mixtures were then subjected a ball milling treatment (0–120 min) prior to their consolidation by SPS. Based on the results with unmilled samples, the milled powders were all processed at 70 MPa, while the selected dwell temperature values for this study were: 700 °C, 800 °C and 950 °C for 25HA-75BG, 50HA-50BG, and 75HA-25BG, respectively. Under such conditions, the relative densities of the three reference samples (t_{BM}= 0 min) fall within a relatively narrow range (90–94 %), and the corresponding residual porosity permits to better highlight the possible influence of the BM treatment on product densification. From the obtained data (Fig. 5), it is seen that sample densities are, depending on the system composition, differently affected by the t_{BM} parameter. For the case of 25HA-75BG, density decreases from 92.9 % to 91.4 % after 30 min process. The corresponding particles coarsening following such treatment (Fig. 1(a)-(b)) apparently inhibits powder consolidation. No further noticeable changes are observed in samples density when the milling process was prolonged to 120 min.

The associate XRD patterns are shown in Fig. 6 while the related microstructural parameters and amounts of each phase, as estimated using the Rietveld analysis, are reported in Table S4. Results clearly evidenced that sintered products from milled powders display a more refined microstructure compared to the unmilled counterpart. In particular, HA crystallite size in the composite samples decreases from > 200 nm (t_{BM}=0 min) down to approximately 60 nm when using
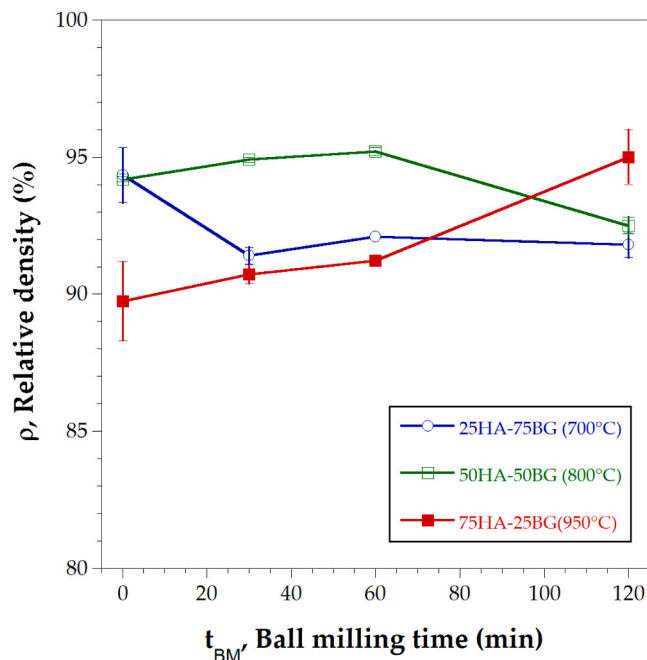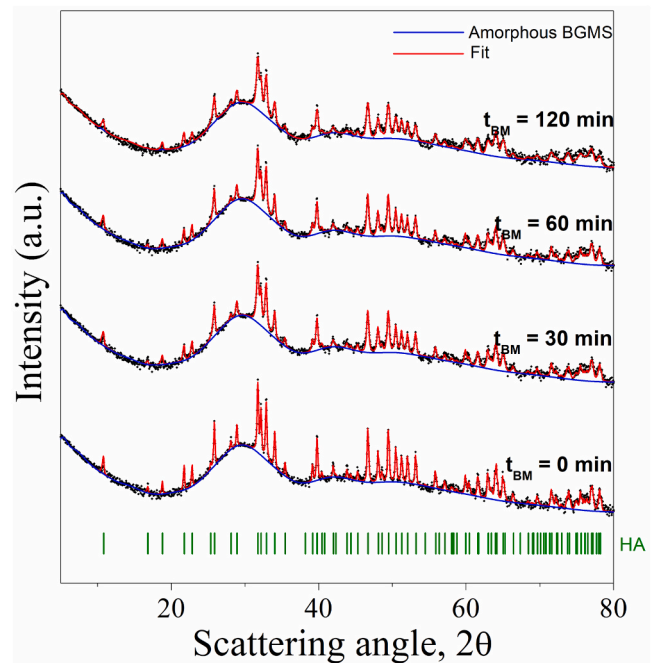

Fig. 6. XRD patterns of bulk 25HA-75BG products obtained SPS (T_D = 700 °C) from unmilled (t_{BM} = 0 min) and milled powders. Black dots are experimental data, and the red line is the calculated fit. Amorphous BGMS10 profile is indicated by the blue full line.

powders mechanically treated for 2 h.

Fig. 5 shows also that, as the weight percentage of BGMS10 was reduced to 50 %, ball milling provided a slight beneficial contribution to powder consolidation, with an increase of the relative density from 94.2 % to 94.9 % at 30 min, and 95.2 % at 60 min

The interfaces formed between the two constituents of the 50HA-50BG mixture are likely responsible for the improved sintering phenomena. In contrast, less dense samples (92.5 %) are obtained when such treatment was extended to 120 min. Two possible motivations were provided by Angioni et al. [18] to justify it. In spite of the positive effect deriving from the interface formation, powder consolidation is made more difficult by the fact that particles processed for 120 min were considerable coarser (Table S1). In addition, using such milled powders, glass devitrification occurred earlier during SPS, with the formation of SiO_2 crystalline phase which, in turn, also contributed to sample densification decrease [18].

In contrast with the behavior displayed by 25HA-75BG and 50HA-50BG systems, Fig. 5 shows the beneficial effects obtained by BM, particularly for longer treatments (60–120 min), when processing the 75HA-25BG mixture, with a marked improvement of the consolidation level from 89.7 % to 95 %. Interestingly, particle coarsening observed in Fig. 1(c)-(d) to take place when milling such powders is expected to inhibit sample densification. Therefore, the correspondingly observed consolidation improvement can be more likely justified by the enhanced HA-BG interfaces formed during the mechanical process. The latter outcome is also responsible for the microstructural changes evidenced by XRD analysis, as shown in Fig. 7 and Table S5. The presence of additional crystalline phases, other than HA, in the sintered unmilled samples is expected, as the T_D value of 950 °C set to consolidate them is above the crystallization temperature of the BGMS10 glass. The two polymorphs of $CaSiO_3$ (α-$CaSiO_3$, Pseudowollastonite, and β-$CaSiO_3$, Wollastonite), with relative amounts of about 3.1 and 4.0 wt %, respectively, were detected. Such phases were also formed when individual glass powders were processed by SPS at dwell temperatures equal of exceeding 850 °C [28]. In addition, tetragonal SiO_2 (t-SiO_2, 8.5 wt %) was also found by XRD in the sintering product. It should be noted that
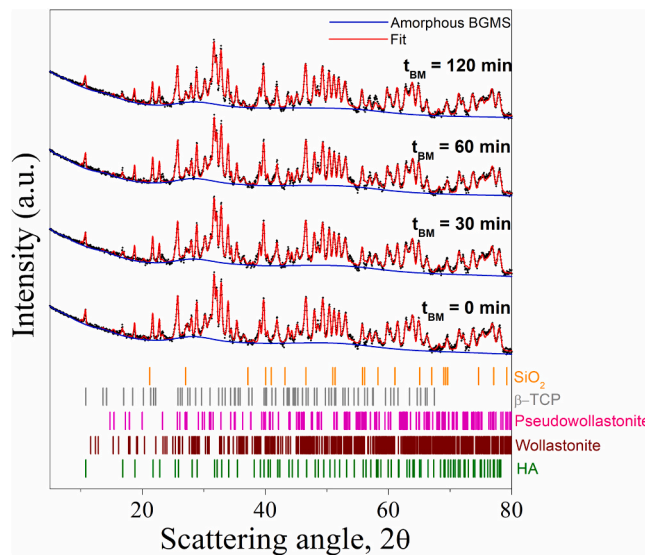

Fig. 5. Density of the three xHA-(1-x)BG products obtained by SPS (P = 70 MPa) as a function of the milling time (t_{BM}).

Fig. 7. XRD patterns of bulk 75HA-25BG products obtained SPS (T_D=950 °C) from unmilled (t_{BM} = 0 min) and milled powders. Black dots are experimental data, and the red line is the calculated fit. Amorphous BGMS10 profile is indicated by the blue full line.

the latter phase was not formed up to 950 °C during heat treatment by SPS of the BGMS10 constituent [28]. On the other hand, SiO_2 was found in 50HA-50BG bulk samples obtained from 2 h milled powders [18]. Very interestingly, the relative content of t-SiO_2 in 75HA-25BG composites monotonically increases up to 13.1 wt % (t_{BM} = 120 min), at the expenses of that of α- (from 3.1 to 1.4 wt %) and β-$CaSiO_3$ (from 4.0 to 2.5 wt %). Moreover, Rietveld analysis also evidenced the presence of a small amount (2.4 wt %) of β-TCP in the sintered specimen, whose content is only modestly affected by the mechanical treatment. Thus, while the amount of apatite in the bulk composite remained roughly constant with milling (slightly less than 70 wt %), crystallites size of this phase is reduced to 82 nm at t_{BM}= 120 min.

3.2.2. Mechanical properties

Micro-indentation tests were conducted on 25HA-75BG (T_D = 700 °C) and 75HA-25BG (T_D = 950 °C) bulk samples to assess their Young's modulus and hardness. The results are presented in Table 1 along with those obtained recently for 50HA-50BG samples (T_D=800 °C) [18]. Data related to nearly full dense BGMS10 [28] and HA [19] samples from unmilled powders are also reported in Table 1, for reference.

As expected, the Young's moduli increase as the fraction of hydroxyapatite in the sample increases; the mechanical properties appear to be further enhanced by longer milling times (t_{BM} = 120 min). An exception is represented by the 50HA-50BG system when the milling time was extended from 30 to 120 min, due the corresponding density decrease, as shown in Table 1 and discussed elsewhere [18]. On the other hand, the 75HA-25BG sample obtained in this work from 120 min milled powders stands out as particularly intriguing in terms of mechanical properties. Indeed, both its Young's modulus and hardness surpass those previously achieved for 50HA-50BG samples and tend to values obtained for nearly full dense pure hydroxyapatite sintered via SPS at significantly higher temperature (1200 °C) [19]. On the other hand, it should be emphasized that making a direct comparison between the mechanical performance of the composites presented here and that of their SPSed counterparts in pure glass [28] or in hydroxyapatite [19] from previous studies is challenging. This is due to the differences in sample densities and process parameters adopted for their production, as seen in Table 1.

Table 1
Young's modulus and hardness of 25HA-75BG and 75HA-25BG bulk samples obtained in this work from differently milled mixtures, as determined through micro-indentation tests. The corresponding sintering temperatures and relative density values are also provided. Literature data relative to nearly full dense samples obtained from pure BGMS10 [28] and HA [19] unmilled powders as well as those related to the 50HA-50BG composite [18] are reported, for comparison.

System	T_D (°C)	t_{BM} (min)	Relative density (%)	Young's Modulus (GPa)	Hardness (Vickers)	Reference
BG	750	0	99.7 ± 0.2	90.92 ± 3.42	671.70 ± 16.60	[28]
25HA-75BG	700	0	94.35 ± 1.0	88.13 ± 2.53	505.30 ± 32.18	This work
		30	91.4 ± 0.3	78.77 ± 3.70	403.33 ± 48.06	
		60	92.1 ± 0.1	88.34 ± 2.18	536.90 ± 44.48	
		120	91.8 ± 0.45	93.91 ± 2.50	596.29 ± 11.70	
50HA-50BG	800	0	94.2 ± 0.1	95.24 ± 2.47	509.88 ± 34.29	[18]
		30	94.7 ± 0.1	122.33 ± 3.58	675.32 ± 38.45	
		120	92.4 ± 0.3	98.01 ± 4.55	683.22 ± 42.21	
75HA-25BG	950	0	89.75 ± 1.45	108.69 ± 7.38	470.59 ± 58.98	This work
		30	90.7 ± 0.4	105.86 ± 4.40	477.27 ± 47.23	
		60	91.2 ± 0.2	98.21 ± 2.79	399.25 ± 33.65	
		120	95.0 ± 1.0	130.06 ± 1.54	725.68 ± 26.18	
HA	1200	0	>99.9	153.00 ± 7.60	771.80 ± 37.20	[19]

3.2.3. Biological behaviour

While the biocompatibility of hydroxyapatite and the favorable biological response observed in prior studies on BGMS10 bioactive glass are well-established [20], it is crucial to assess the cytotoxicity of the composites consolidated using the advanced SPS technique. Furthermore, it is noteworthy to emphasize the limited available literature on the biological performance of biocompatible materials fabricated using this technique.

In the present study, cytotoxicity was evaluated on 25HA-75BG, 50HA-50BG, and 75HA-25BG bulk samples obtained by SPS from unmilled and 30 min milled powders (cf. Table 1). Indirect tests on the samples' eluates were conducted using the alamar-Blue® kit, a versatile metabolic dye. Alamar-Blue® is a redox indicator that quantitatively measures cell proliferation. As cells proliferate, metabolic activity increases, resulting in a reduction in the surrounding culture medium, while growth inhibition creates an oxidizing environment. Reduction leads to a color change in the alamar-Blue® indicator from non-fluorescent (λ_{max} = 600 nm, blue) to fluorescent (λ_{max} = 570 nm, red). The proposed mechanism for the dye's detection of living cells involves reduction based on metabolic activity through reactions in the respiratory chain [30]. Cell viability was assessed after 24 and 72 h of culture in the sample extracts. The obtained results, presented in Fig. 8, confirm the non-cytotoxic nature of all the composite samples. In addition, the 30 min mechanical treatment apparently does not cause any negative consequence in this regard.

4. Summary and conclusions

When HA and BGMS10 glass powders are co-milled up to 2 h prior to their consolidation by SPS, compositional, microstructural, mechanical, and biological characteristics of the resulting bulk products depend on the mechanical treatment conditions, whose effects are found to be
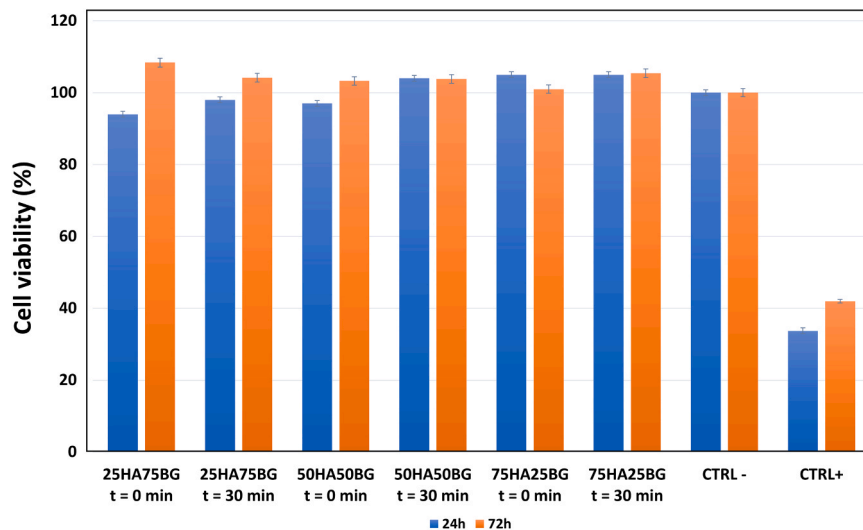
Fig. 8. Results of the alamar-Blue® test of MLOY04 cells cultured in extracts from the 25HA-75BG, 50HA-50BG, and 75HA-25BG samples (t_{BM}=0 and 30 min) after 24 and 72 h.

strictly related to the specific composite formulation. The most relevant modifications induced by BM in the processing powders concern particles agglomeration (for 50 wt % or higher amounts of HA) or comminution (composite mixtures richer in BG), surface area increase (from 5.6-7.2 to 16.1–19.3 m^2 g^{-1}), apatite crystallites refinement (from > 200 nm to 44–53 nm), as well as HA-BG interface enhancement. As for the sintering behaviour of the resulting mixtures, such changes produced beneficial effects in the 75HA-25BG system, hindered the consolidation of 25HA-75BG powders, while an intermediate situation is encountered when processing 50HA-50BG samples. Very important, a more refined microstructure is obtained in SPS products deriving from milled powders, with the HA crystallite size reduction from >200 nm (t_{BM}=0 min) down to 60 nm (25HA-75BG) and 88 nm (75HA-25BG) after 2 h treatment.

Regardless the milling time conditions, only modest changes (in the range 12.3–13.3 wt %) are obtained in the content of residual amorphous phase of 75HA-25BG samples processed by SPS at 950 °C, i.e., above the crystallization temperature of the BMS10 glass. In contrast, the relative amount of t-SiO_2 correspondingly formed raised from 8.5 (unmilled) to 13.1 wt % (t_{BM} = 120 min), at the expenses of that of α-(from 3.1 to 1.4 wt %) and β-$CaSiO_3$ (from 4.0 to 2.5 wt %). The samples richer in HA and subjected to a 2 h milling treatment also exhibit superior mechanical properties, with Young's modulus and Vickers hardness of about 130 GPa and 726, respectively, not so different to values measured for fully dense 100 %HA products obtained by SPS at higher temperatures from the same powders.

Finally, despite the HA-BG formulations, the SPS conditions, and the resulting microstructural characteristics are rather diverse, the biological test conducted on the bulk composite samples produced from either untreated or 30 min milled mixtures evidenced that they are all noncytotoxic.

The obtained results make the developed novel composites very promising for their utilization in regenerative medicine.

Funding

Declaration of Competing Interest

The authors declare that they have no known competing financial interests or personal relationships that could have appeared to influence the work reported in this paper.

Acknowledgements

Appendix A. Supporting information

Supplementary data associated with this article can be found in the online version at doi:10.1016/j.jeurceramsoc.2023.07.079.

References

[1] S.V. Dorozhkin, Calcium orthophosphate bioceramics, Ceram. Int. 41 (10) (2015) 13913–13966, https://doi.org/10.1016/j.ceramint.2015.08.004.

[2] J.R. Jones, Review of bioactive glass: from Hench to hybrids, Acta Biomater. 9 (1) (2013) 4457–4486, https://doi.org/10.1016/j.actbio.2012.08.023.

[3] J.C. Knowles, W. Bonfield, Development of a glass reinforced hydroxyapatite with enhanced mechanical properties. The effect of glass composition on mechanical properties and its relationship to phase changes, J. Biomed. Mater. Res. 27 (12) (1993) 1591–1598, https://doi.org/10.1002/jbm.820271217.

[4] J.D. Santos, R.L. Reis, F.J. Monteiro, J.C. Knowles, G.W. Hastings, Liquid phase sintering of hydroxyapatite by phosphate and silicate glass additions: structure and properties of the composites, J. Mater. Sci. Mater. Med. 6 (1995) 348–352, https://doi.org/10.1007/BF00120303.

[5] J.D. Santos, P.L. Silva, J.C. Knowles, S. Talal, F.J. Monteiro, Reinforcement of hydroxyapatite by adding P_2O_5-CaO glasses with Na_2O, K_2O and MgO, J. Mater. Sci. Mater. Med. 7 (1996) 187–189, https://doi.org/10.1007/BF00121259.

[6] L.J. Jha, J.D. Santos, J.C. Knowles, Characterization of apatite layer formation on P_2O_5-CaO, P_2O_5-CaO-Na_2O, and P_2O_5-CaO-Na_2O-Al_2O_3 glass hydroxyapatite composites, J. Biomed. Mater. Res. 31 (4) (1996) 481–486, https://doi.org/10.1002/(sici)1097-4636(199608)31:4%3C481::aid-jbm7%3E3.0.co;2-h.

[7] D. Tanaskovic, B. Jokic, G. Socol, A. Popescu, I.N. Mihailescu, R. Petrovic, D.J. Janackovic, Synthesis of functionally graded bioactive glass-apatite multistructures on Ti substrates by pulsed laser deposition, Appl. Surf. Sci. 254 (4) (2007) 1279–1282, https://doi.org/10.1016/j.apsusc.2007.08.009.

[8] D. Bellucci, A. Sola, V. Cannillo, Bioactive glass-based composites for the production of dense sintered bodies and porous scaffolds, Mater. Sci. Eng. C 33 (4) (2013) 2138–2151, https://doi.org/10.1016/j.msec.2013.01.029.

[9] D. Bellucci, A. Sola, A. Anesi, R. Salvatori, L. Chiarini, V. Cannillo, Bioactive glass/hydroxyapatite composites: mechanical properties and biological evaluation, Mater. Sci. Eng. C 51 (2015) 196–205, https://doi.org/10.1016/j.msec.2015.02.041.

[10] D. Bellucci, L. Desogus, S. Montinaro, R. Orrù, G. Cao, V. Cannillo, Innovative hydroxyapatite/bioactive glass composites processed by spark plasma sintering for bone tissue repair, J. Eur. Ceram. Soc. 37 (4) (2017) 1723–1733, https://doi.org/10.1016/j.jeurceramsoc.2016.11.012.

[11] D. Bellucci, R. Salvatori, A. Anesi, L. Chiarini, V. Cannillo, SBF assays, direct and indirect cell culture tests to evaluate the biological performance of bioglasses and bioglass-based composites: Three paradigmatic cases, Mater. Sci. Eng. C 96 (2019) 757–764, https://doi.org/10.1016/j.msec.2018.12.006.

[12] N. Pinchuk, O. Parkhomey, O. Sych, In vitro investigation of bioactive glass-ceramic composites based on biogenic hydroxyapatite or synthetic calcium phosphates, Nanoscale Res. Lett. 12 (1) (2017) 111, https://doi.org/10.1186/s11671-017-1895-1.

[13] S. Mondal, G. Hoang, P. Manivasagan, M.S. Moorthy, T.P. Nguyen, T.T. Vy Phan, H.H. Kim, M.H. Kim, S.Y. Nam, J. Oh, Nano-hydroxyapatite bioactive glass composite scaffold with enhanced mechanical and biological performance for tissue engineering application, Ceram. Int. 44 (13) (2018) 15735–15746, https://doi.org/10.1016/j.ceramint.2018.05.248.

[14] Z. Catalgol, Sintering effect on borosilicate glass-bovine hydroxyapatite composites, J. Aust. Ceram. Soc. 55 (4) (2019) 1075–1079, https://doi.org/10.1007/s41779-019-00320-y.

[15] J.A. Rincón-López, J.A. Hermann-Muñoz, D.A. Fernández-Benavides, A. David, A. L. Giraldo-Betancur, J.M. Alvarado-Orozco, J. Muñoz-Saldaña, Isothermal phase transformations of bovine-derived hydroxyapatite/bioactive glass: a study by design of experiments, J. Eur. Ceram. Soc. 39 (4) (2019) 1613–1624, https://doi.org/10.1016/j.jeurceramsoc.2018.11.021.

[16] M. Luginina, D. Angioni, S. Montinaro, R. Orrù, G. Cao, R. Sergi, D. Bellucci, V. Cannillo, Hydroxyapatite/bioactive glass functionally graded materials (FGM) for bone tissue engineering, J. Eur. Ceram. Soc. 40 (13) (2020) 4623–4634, https://doi.org/10.1016/j.jeurceramsoc.2020.05.061.

[17] M. Lakrat, M. Jabri, M. Alves, M.H. Fernandes, L.L. Ansari, C. Santos, E. M. Mejdoubi, Three-dimensional nano-hydroxyapatite sodium silicate glass composite scaffold for bone tissue engineering - a new fabrication process at a near-room temperature, Mater. Chem. Phys. 260 (2021), 124185, https://doi.org/10.1016/j.matchemphys.2020.124185.

[18] D. Angioni, R. Orrù, G. Cao, S. Garroni, D. Bellucci, V. Cannillo, Bioactivity enhancement by a ball milling treatment in novel bioactive glass-hydroxyapatite composites produced by spark plasma sintering, J. Eur. Ceram. Soc. 43 (3) (2023) 1220–1229, https://doi.org/10.1016/j.jeurceramsoc.2022.10.077.

[19] A. Cuccu, S. Montinaro, R. Orrù, G. Cao, D. Bellucci, A. Sola, V. Cannillo, Consolidation of different Hydroxyapatite powders by SPS: optimization of the sintering conditions and characterization of the obtained bulk products, Ceram. Int. 41 (1) (2015) 725–736, https://doi.org/10.1016/j.ceramint.2014.08.131.

[20] D. Bellucci, V. Cannillo, A novel bioactive glass containing strontium and magnesium with ultra-high crystallization temperature, Mater. Lett. 213 (2018) 67–70, https://doi.org/10.1016/j.matlet.2017.11.020.

[21] D. Bellucci, A. Sola, V. Cannillo, Low temperature sintering of innovative bioactive glasses, J. Am. Ceram. Soc. 95 (2012) 1313–1319, https://doi.org/10.1111/j.1551-2916.2012.05100.x.

[22] O. Bretcanu, X. Chatzistavrou, K. Paraskevopoulos, R. Conradt, I. Thompson, A. Boccaccini, Sintering and crystallisation of 45S5 Bioglass® powder, J. Eur. Ceram. Soc. 29 (2009) 3299–3306, https://doi.org/10.1016/j.jeurceramsoc.2009.06.035.

[23] S. Kargozar, M. Montazerian, E. Fiume, F. Baino, Multiple and promising applications of strontium (Sr)-containing bioactive glasses in bone tissue engineering, Front Bioeng. Biotechnol. 7 (2019) 161, https://doi.org/10.3389/fbioe.2019.00161.

[24] I. Cacciotti, Bivalent cationic ions doped bioactive glasses: the influence of magnesium, zinc, strontium and copper on the physical and biological properties, J. Mater. Sci. 52 (2017) 8812–8831, https://doi.org/10.1007/s10853-017-1010-0.

[25] L. Lutterotti, R. Ceccato, R. Dal Maschio, E. Pagani, Quantitative analysis of silicate glass in ceramic materials by the Rietveld method, Mater. Sci. Forum 87 (1998) 278–281, https://doi.org/10.4028/www.scientific.net/MSF.278-281.87.

[26] M. Baricco, T.A. Baser, G. Enzo, G. Vaughan, A.R. Yavari, Analysis of crystallization behavior of Fe48Cr15Mo14Y2C15B6 bulk metallic glass by synchrotron radiation, J. Mater. Res. 23 (2008) 2166–2173, https://doi.org/10.1557/JMR.2008.0264.

[27] F.L. Matthews, R. Rawlings, Composite Materials: Engineering and Science, Chapman & Hall, Great Britain, 1994.

[28] D. Angioni, R. Orrù, G. Cao, S. Garroni, A. Iacomini, D. Bellucci, V. Cannillo, Spark plasma sintering, mechanical and in-vitro behavior of a novel Sr- and Mg-containing bioactive glass for biomedical applications, J. Eur. Ceram. Soc. 42 (4) (2022) 1776–1783, https://doi.org/10.1016/j.jeurceramsoc.2021.11.061.

[29] W. Oliver, G. Pharr, An improved technique for determining hardness and elastic modulus using load and displacement sensing indentation experiments, J. Mater. Res. 7 (1992) 1564–1583, https://doi.org/10.1557/JMR.1992.1564.

[30] S.L. Voytik-Harbin, A.O. Brightman, B. Waisner, C.H. Lamar, S.F. Badylak, Application and evaluation of the alamarBlue assay for cell growth and survival of fibroblasts, Vitr. Cell Dev. Biol. Anim. 34 (3) (1998) 239–246, https://doi.org/10.1007/s11626-998-0130-x.